PHYSICAL REVIEW C **80**, 014602 (2009)

Break-up fragment topology in statistical multifragmentation models

Ad. R. Raduta

NIPNE, Bucharest-Magurele, POB-MG6, Romania and

Institut de Physique Nucleaire, Universite Paris-Sud 11, CNRS/IN2P3, F-91406 Orsay cedex, France

(Received 20 November 2008; revised manuscript received 30 March 2009; published 8 July 2009)

Break-up fragmentation patterns together with kinetic and configurational energy fluctuations are investigated in the framework of a microcanonical model with fragment degrees of freedom over a broad excitation energy range. As long as fragment partitioning is approximately preserved, energy fluctuations are found to be rather insensitive to both the way in which the freeze-out volume is constrained and the trajectory followed by the system in the excitation-energy–freeze-out volume space. Due to hard-core repulsion, the freeze-out volume is found to be populated nonuniformly, its highly depleted core giving the source a bubble-like structure. The most probable localization of the largest fragments in the freeze-out volume may be inferred experimentally from their kinematic properties, largely dictated by Coulomb repulsion.

DOI: 10.1103/PhysRevC.80.014602 PACS number(s): 25.70.Pq, 64.60.an, 24.10.Pa, 25.70.Mn

I. INTRODUCTION

For more than two decades, nuclear multifragmentation has benefited from a constant scientific interest whose main motivation is the observation of a (liquid-gas-like) phase transition at subatomic scale [1,2].

Relying on the presumptive existence of an equilibrated break-up stage in the simultaneous multiparticle decay of excited nuclei, statistical models with cluster degrees of freedom [3–7] represent particularly useful tools for the characterization of the equilibrated state of the source and, not less importantly, the study of the associated thermodynamics. The remarkable advantage of realistically incorporating most properties of bound and continuum states via empirical parametrizations of cluster energies or level densities explains their ability to describe well a wealth of experimental data produced over a broad energetic domain.

It was demonstrated that experimental data corresponding to a well-defined equilibrated source may be described by a unique solution of such a statistical model [8,9]. It is nevertheless not true that the different statistical models converge to the same equilibrated source if the analysis is done by exclusively considering experimental (after-burner) information [10]. This is partly due to the different thermodynamical constraints imposed on the employed statistical ensembles or mathematical tricks designed to simplify the partition function or speed up the simulation and, to a much larger extent, to the differences in the break-up fragment definition.

The aim of the present work is to contribute to a deeper understanding of the break-up stage of the multifragmentation decay as ruled by statistical laws. For this reason, contributions from dynamics (as radial collective flow) and sequential particle evaporations from primary fragments will be referred to only tangentially, despite that over an important region of the considered energy domain they play an important role. For the same reason we will ignore also eventual fragment recombination subsequent to the break-up, thoroughly considered by some authors [11,12]. More precisely, we want to see

(i) whether fluctuations of different energetic degrees of freedom are mainly dictated by the localization of the decay event into the phase diagram or, conversely, by the dominant fragmentation modes,
(ii) whether break-up nuclear matter distribution is uniform, and, if not,
(iii) whether it is possible to trace the nonhomogeneities from experimentally accessible data.

The paper is organized as follows: Sec. II offers a brief review of the statistical models of multifragmentation with a special focus on the microcanonical ones employed here; Sec. III investigates the sharing of a system's available energy among different degrees of freedom and the sensitivity of the energy fluctuations to the system phase properties and fragment partition; Sec. IV focuses on break-up patterns and the extent to which these may be inferred from kinetic energy distributions. Modifications of fragment charge distributions brought by considering that, at variance with the standard break-up picture, primary fragments interact through nuclear forces are also addressed in Sec. IV. Conclusions are drawn in Sec. V.

II. STATISTICAL TREATMENT OF MULTIFRAGMENTATION

Under the equilibrium hypothesis, statistical models reduce the physical problem under study to the estimation of the number of microscopic states compatible with the thermodynamical macroscopic constraints. This implies that assuming that it is possible to write down the mathematical expression of the statistical weight of a configuration W_C in the appropriate statistical ensemble, all the thermodynamic quantities may be calculated out of the characteristic partition sum

$$\mathcal{Z} = \sum_C W_C, \tag{1}$$

while any ensemble-averaged observable X may be expressed as

$$\langle X_C \rangle = \frac{\sum_C W_C X_C}{\sum_C W_C}. \quad (2)$$

While for relatively large extensive systems, thermodynamical properties are not sensitive to the way in which the statistical ensemble is defined, when dealing with small systems, as the nuclear ones, it is important to choose the most appropriate replica of the physical phenomenon. Because of the lack of any thermal or chemical potential reservoirs in the case of isolated multifragmenting nuclei, the microcanonical ensemble is recommended as the most reasonable choice [3,13,14]. In this case, it is obvious that the conserved quantities are the total proton (Z) and neutron ($A - Z$) numbers, the total energy (E), total momentum ($\mathbf{P}$), and, eventually, total angular momentum ($\mathbf{L}$). The freeze-out volume (V) may be considered as either fixed or fluctuating.

Defining a generic break-up configuration by the isotopic, internal, and translational properties of each fragment, $C = \{A_1, Z_1, \epsilon_1, \mathbf{r}_1, \ldots, A_{N_C}, Z_{N_C}, \epsilon_{N_C}, \mathbf{r}_{N_C}\}$, one gets for the statistical weight of the constant volume ensemble the equation [6]

$$W_C(A, Z, E, V) \propto \frac{1}{N_C!}\Omega \prod_{n=1}^{N_C} \left(\frac{\rho_n(\epsilon_n)}{h^3} (m A_n)^{3/2} \right) \times \frac{2\pi}{\Gamma[3/2(N_C - 2)]} \frac{1}{\sqrt{(\det I)}} \times \frac{(2\pi K)^{3/2 N_C - 4}}{(mA)^{3/2}}, \quad (3)$$

where I is the moment of inertia, K is the thermal kinetic energy, and $\Omega = \chi V^{N_C}$ stands for the free volume or, equivalently, accounts for interfragment interaction in the hard-core idealization. From Eq. (3) it is straightforward to calculate the statistical weight of a microcanonical ensemble with fluctuating volume as

$$\mathcal{W}_C(A, Z, E, \lambda) = \int W_C(A, Z, E, V) \exp(-\lambda V)\, dV. \quad (4)$$

It is worthwhile to mention at this point that working under a fixed total energy constraint, it results that the thermal kinetic energy, a key thermodynamic quantity related to the temperature through $T^{-1} = (\partial S/\partial E) = 1/W(A, Z, E, V) \partial W(A, Z, E, V)/\partial E$, is determined by the amount of energy available after extracting from the source excitation the costs of fragment formation $\sum_i B_i$, fragment internal excitation $\sum_i \epsilon_i$, and mutual fragment interaction $\sum_{i<j} V_{ij}$,

$$K = E_{\rm ex} - Q - \sum_i \epsilon_i - \sum_{i<j} V_{ij}. \quad (5)$$

This implies that also the fluctuations of K are strongly dependent on the fluctuations of the other three energetic degrees of freedom, as we shall see later on.

The results discussed hereafter were obtained in the framework of the microcanonical model of multifragmentation (MMM) [6] in the case of the medium size nucleus (130,60) within the commonly accepted scenario according to which the break-up fragments do not interact otherwise than via Coulomb forces. The consequences of considering in the spirit of Refs. [11,12,15] that break-up fragments also feel the nuclear proximity potential are discussed only with respect to fragment charge distributions, for the sake of completeness. Despite the particular choices regarding the model and the nucleus, the results are considered generic for the statistical break-up of multifragmenting nuclei.

Two arbitrary paths in the phase diagram have been considered: a constant volume path $V = 6V_0$ and one along which the *average* volume increases with excitation energy. The motivation of choosing a constant volume path is twofold. First, it reproduces the fixed freeze-out volume statistical constraint that has been used for treating multifragmentation over almost two decades, and second, it accounts for the belief that the freeze-out volume (average) value does not change significantly as the source excitation energy increases. Twofold also is the motivation of choosing the second path. First, it cancels the statistical constraint of constant volume, and second, it accounts for a freeze-out volume whose (average) value may increase with energy, as recent analyses of experimental data indicate [16,17]. In this last case, the average freeze-out volume increases from $3.5V_0$ at 2 MeV/nucleon to about $10.4V_0$ at 14 MeV/nucleon, as indicated in the inset of Fig. 1. Even more importantly, the two paths differ by the regions of the system phase diagram they explore. Thus, following the evolution of the heat capacity,

$$C^{-1} = -T^2 \left(\frac{\partial^2 S}{\partial E^2} \right) = 1 - T^2 \frac{1}{W(A, Z, E, V)} \frac{\partial^2 W(A, Z, E, V)}{\partial E^2} = 1 - T^2 \left\langle \frac{\left(\frac{3}{2}N - 4\right)\left(\frac{3}{2}N - 5\right)}{K^2} \right\rangle, \quad (6)$$

plotted in Fig. 1 as a function of excitation energy, one may notice that the constant volume path is supracritical, while the increasing average-volume path crosses the phase coexistence

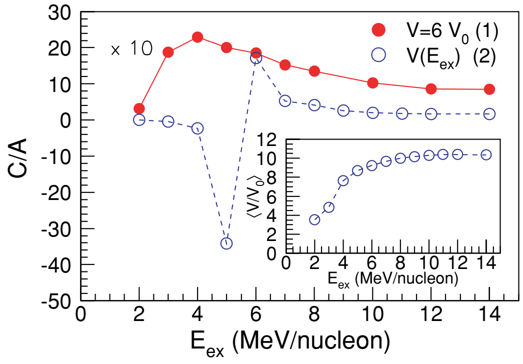

FIG. 1. (Color online) Heat capacity vs source excitation energy for the multifragmenting nucleus (130,60) which evolves through the phase space following (1) a constant freeze-out volume $V = 6V_0$ path or (2) a path characterized by an average freeze-out volume that increases with the excitation, as indicated in the inset.

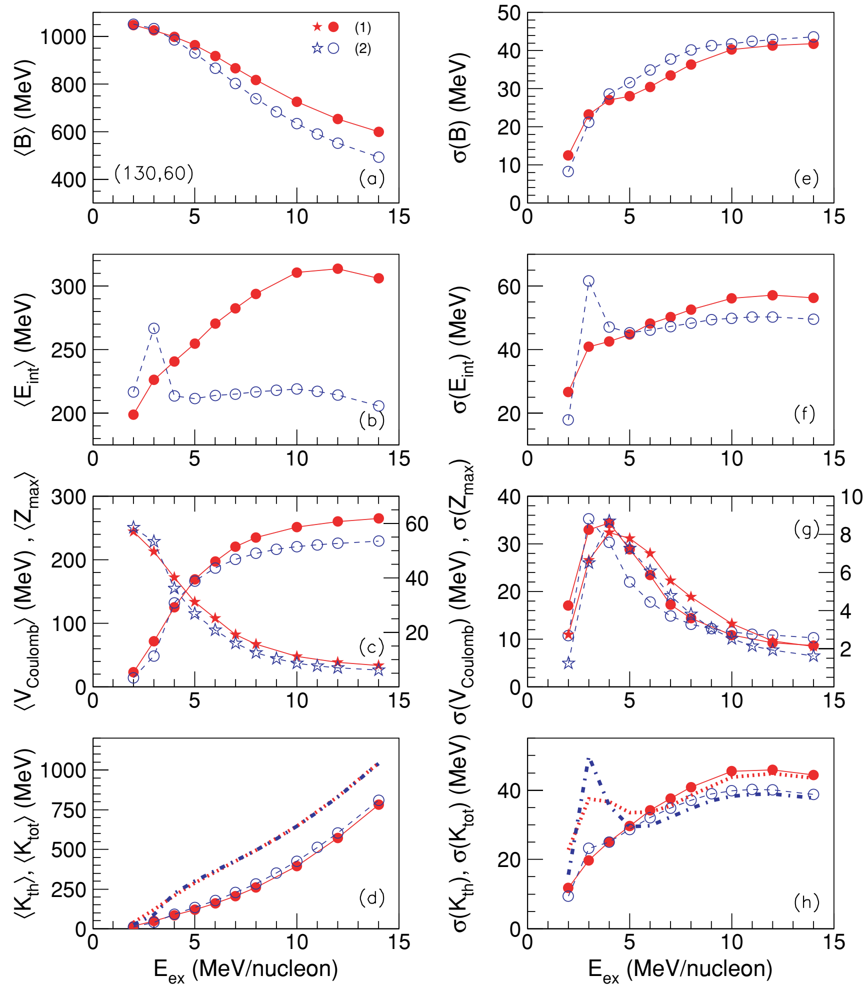

FIG. 2. (Color online) Evolution with source excitation energy of mean (left column) and rms (right column) values of total binding energy (a) and (e), total fragment internal excitation (b) and (f), Coulomb fragment-fragment interaction (c) and (g), and thermal kinetic energy (d) and (h), corresponding to the break-up stage of the (130, 60) multifragmenting nucleus. The considered states along a constant volume $V = 6V_0$ (1) and an average volume increasing with excitation (2) paths are represented by solid and open circles. The open and solid stars in (c) and (g) depict the excitation energy dependence of the largest fragment in each decay event. The dashed lines in (d) and (h) stand for total fragment kinetic energy.

region. Phase coexistence is signaled by negative values of the heat capacity.

III. ENERGY SHARING AT BREAK-UP: AVERAGE AND RMS VALUES

Figures 2(a)–2(d) present, respectively, the average values of the total fragment binding energy, internal excitation, Coulomb interaction, and thermal kinetic energy together with their rms values [Figs. 2(e)–2(h)] corresponding to the break-up stage of a (130,60) nucleus whose excitation energy ranges from 2 to 14 MeV/nucleon along the two considered trajectories. Distributions of the mean charge of the largest fragment and its rms are superimposed on the Figs. 2(c) and 2(g) with full and open stars. Dashed lines in Figs. 2(d) and 2(h) indicate how the total fragment kinetic energy, a quantity experimentally accessible, behaves with respect to source excitation.

One can see that, irrespective of the considered path, the more and more advanced fragmentation allowed by an increasing source energy, suggested by a rapidly decreasing $Z_{\max}$, leads to a monotonic diminish of the total binding energy and a monotonic increase of the total Coulomb interaction energy. The total binding energy decrease is due to the increasing fragment surfaces, while the increase of the total Coulomb interaction energy is explained by an increasingly uniform occupation of the volume. While the curves corresponding to the two considered paths diverge with excitation, they are still not far from one another, as for a given $E_{\rm ex}$ their values differ by at most 20% in the considered energy domain. In contrast with this, the amount of energy dissipated in fragment internal excitation has a more complex evolution, and the relative difference among the values obtained along the two paths reaches 50% at $E_{\rm ex} = 14$ MeV/nucleon. Nevertheless, the evolution and relative magnitude of the above quantities are such that the kinetic energy increases monotonically, as one would expect [see Fig. 2(d)].

The right-side panels of Fig. 2 present the energy fluctuations and indicate that, as more and more fragment partitions are possible with the increasing energy, $\sigma(B)$ and $\sigma(E_{\rm int})$ rise as well. Very interestingly, $\sigma(V_C)$ augments up to 4 MeV/nucleon and then decreases. The positive slope region corresponds to the energy domain where configurations containing one heavy residue are dominant. The negative slope interval corresponds to a regime of rather advanced fragmentation which allows for a more uniform population of the freeze-out volume. As one may notice, the peak of $\sigma(V_C)$ corresponds roughly to the peak of $\sigma(Z_{\max})$ [full and open stars in the Fig. 2(g)] and indicates that the largest fragment

$Z_{\max}$ dictates the geometrical arrangement of fragments and, finally, the Coulomb energy.

Another observation is that because the reduction of the Coulomb energy fluctuation is less significant than the increase of the internal excitation and binding energy fluctuations, $\sigma(K_{\text{th}})$ increases monotonically. Nevertheless, analyzing the experimentally accessible fragment total kinetic energy distribution, one notes a peak at 3 MeV/nucleon, as the consequence of summing up the peaked $\sigma(V_C)$ with the monotonically increasing $\sigma(K_{\text{th}})$ [Fig. 2(h)].

But the first important result is that fluctuations of kinetic and configurational energetic channels prove rather insensitive to both freeze-out volume constraints and the trajectory followed by the system into the excitation-energy–freeze-out volume plane, provided that the fragmentation pattern is preserved. The result is even more striking as the two considered trajectories explore different regions of the phase diagram.

IV. FRAGMENTATION PATTERNS AND NUCLEAR MATTER RADIAL DISTRIBUTIONS

The break-up fragmentation pattern corresponding to 4 MeV/nucleon excitation energy, where the largest fluctuations in $\sigma(Z_{\max})$ and $\sigma(V_C)$ manifest themselves, is illustrated in the Fig. 3(a), while Fig. 4(a) presents the fragmentation pattern obtained at a slightly higher source excitation, 6 MeV/nucleon. As no sensitivity was found to the way in which the freeze-out volume in constrained, from here on we shall consider only the case corresponding to $V = 6V_0$.

One can see that at $E_{\text{ex}} = 4$ MeV/nucleon, the dominant fragmentation mode is characterized by a residue representing 80% of the total system, but multifragmentation configurations are already possible. For instance, configurations characterized by two intermediate size fragments ($Z_{\max} \approx 30$ and $Z_{\max 2} \approx 20$), though five times less probable than the most probable fragmentation mode, are nevertheless frequent enough to induce a quite flat $Y(Z_{\max})$. The diversity of fragmentation modes translated in broad $Z_{\max}$ and $Z_{\max 2}$ distributions persists at 6 MeV/nucleon, but it is no longer possible to identify a close competition among different fragmentation patterns. This means that there are no more distinct ways of filling up the available volume, whose coexistence leads to large fluctuation of the Coulomb energy.

We recall at this point that fragmentation patterns are nevertheless very sensitive to the break-up fragment definition or modeling of the break-up stage itself. If, for instance, one sticks to the noninteracting break-up fragments scenario but considers that, in agreement with Thomas-Fermi calculations, excited nuclei at freeze-out are diluted, the fragment charge distribution will be settled by the competition between the reduced free volume and the augmented thermal kinetic energy. The same qualitative situation is reached if not the fragment densities but their internal excitations are modified. If, for example, one adopts for the nuclear level density an expression that leads to lower fragment internal excitation, in view of Eq. (5), K_{th} will increase, favoring an increased reaction products multiplicity. In turn, this last quantity, by making possible a more uniform population of the freeze-out volume characterized by a larger V_C, will tend to diminish K_{th}.

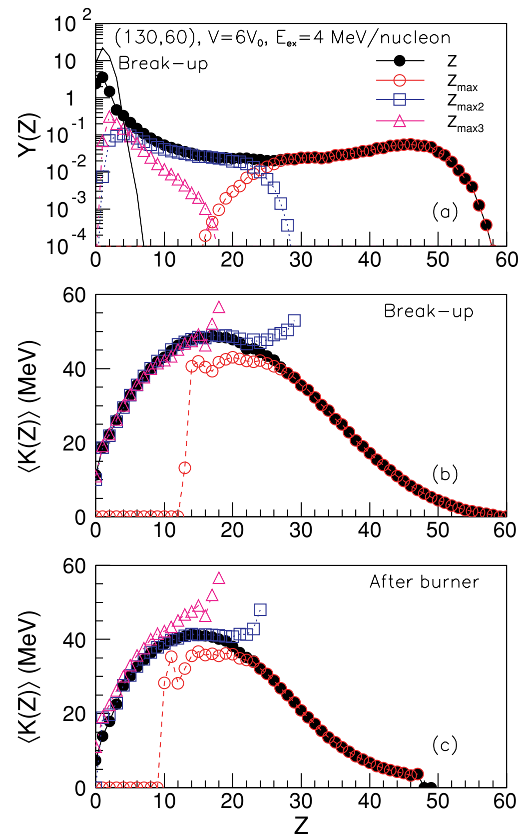

FIG. 3. (Color online) Charge distributions (a) and distributions of average kinetic energy as a function of fragment charge [(b) and (c)] corresponding to the multifragmentation of the (130,60) nucleus with $V = 6V_0$ and $E_{\text{ex}} = 4$ MeV/nucleon. (a) and (b) depict break-up stage results, while after-burner data are illustrated in (c). Solid circles stand for all fragments; open circles, open squares, and open triangles stand, respectively, for the largest, second largest, and third largest fragment in each event. The solid line in (a) corresponds to the break-up fragment charge distribution obtained under the assumption that break-up fragments interact not only through repulsive hard-core and Coulomb potentials but also via proximity potentials.

Much dramatic modifications are expected if one considers that break-up fragments interact not only via repulsive Coulomb but also via attractive nuclear proximity potentials. This conceptually different approach is mainly justified by the fact that for break-up volumes of the order of a few V_0 the distances between fragment surfaces may be lower than $\sim$1 fm. This situation has been discussed recurrently in Refs. [11,12,15], together with break-up fragment subsequent recombination, and shown to lead to an increased productivity of light and heavy fragments at the cost of the intermediate ones. As recombination, which occurs if two fragments approach each other during the Coulomb propagation, acts in the sense of washing-out the statistical properties of break-up fragment formation, here we shall restrict ourselves to comment exclusively on the consequences of modifying fragment energetics.

It is relatively easy to anticipate from Eq. (5) that by considering an extra attractive potential, one will obtain an increase in thermal kinetic energy and reaction products

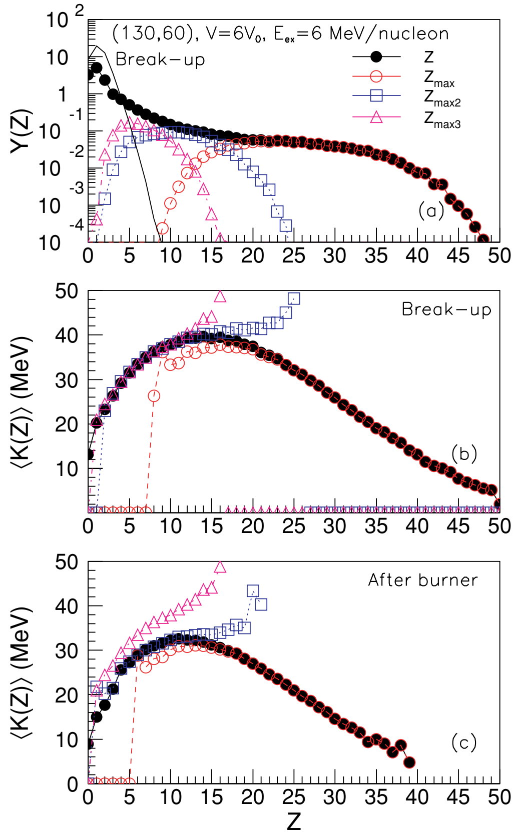

FIG. 4. (Color online) Same as Fig. 3, but for the multifragmentation of the (130,60) nucleus with $V = 6V_0$ and $E_{ex} = 6$ MeV/nucleon.

multiplicity. The confirmation is given by the solid curves Figs. 3(a) and 4(a) obtained in the case in which the nuclear interactions are implemented as in Ref. [11]. In both situations, one may notice a dramatic enhancement of the light cluster multiplicity and the total suppression of fragments with $Z \geqslant 10$. These steep $Y(Z)$ distributions and the evolution of their slopes with source excitation may be reconciled with experimental data if and only if one assumes that final fragment formation is dominated by post-break-up dynamics (including collective flow) and multiparticle correlation [12]. If this were the case, the freeze-out would occur much later than the break-up. The complete modeling of this process is nevertheless a challenging task that goes beyond the goal of the present paper.

In addition to charge distributions, fragment average kinetic energy distributions represent robust and directly accessible experimental information and make up a key ingredient in the standard procedure of identifying the statistically equilibrated source by confrontation with predictions of statistical models [8,9]. The Figs. 3(b), 3(c), 4(b), and 4(c) depict the average kinetic energy distributions of primary and, respectively, cold fragments corresponding to the same source (130,60) with $V = 6V_0$ and $E_{ex} = 4$ and 6 MeV/nucleon. The inclusive distributions are plotted with full circles, while distributions corresponding to the largest, second largest, and third largest fragment are plotted with open circles, squares and triangles. Collective radial flow is set to zero to keep fragment statistical properties unaffected.

Fragment average kinetic energy distributions are qualitatively similar for the two source excitations. As one may notice, the maximum value of 49 (42) MeV reached by the primary (asymptotic) $\langle K(Z)\rangle|_{4\ \mathrm{MeV/nucleon}}$ distribution exceeds by 25% (30%) the maximum value obtained by the corresponding $\langle K(Z)\rangle|_{6\ \mathrm{MeV/nucleon}}$ distribution. This result is in apparent contrast with what one would expect given the increase of 57% of the total Coulomb energy over the considered energy domain, though it may be understood by taking into account the much stronger increase in the total number of reaction products [18].

A common and interesting feature is present in the charge domain where the $\langle K(Z)\rangle$ distributions reach their maximum. Thus, the break-up and asymptotic average kinetic energies of the largest fragment are systematically smaller than the average kinetic energies of the second largest fragment, which are, in their turn, smaller than the ones corresponding to the third largest fragment. This result has been already pointed out by the INDRA Collaboration in the case of Xe + Sn at 32 MeV/nucleon and Gd + U at 36 MeV/nucleon reactions [19] and shown to diminish with the source excitation energy, in perfect agreement with the present results. Taking into account that fragment kinetic energies are to a large extent dictated by Coulomb, it becomes obvious that in analyzing them, one may get information on the most probable fragment position at break-up. Having the same dependence as Coulomb on fragment mass and distance from the freeze-out volume center, radial collective flow, if present, would enhance this shift. If this reasoning is correct, it means that the larger a fragment is, the closer it is produced to the freeze-out volume center.

The answer to this issue is offered by Fig. 5, where radial probability distributions of different size fragments corresponding to the break-up stage of the (130,60) source with $V = 6V_0$ and $E_{ex} = 4$ MeV/nucleon are plotted. As a first general remark, one may say that the probability to create a fragment inside the freeze-out volume, whatever its size, is highly nonuniform and strongly diminishes in the core region. Moreover, heavy fragments are localized preferentially toward

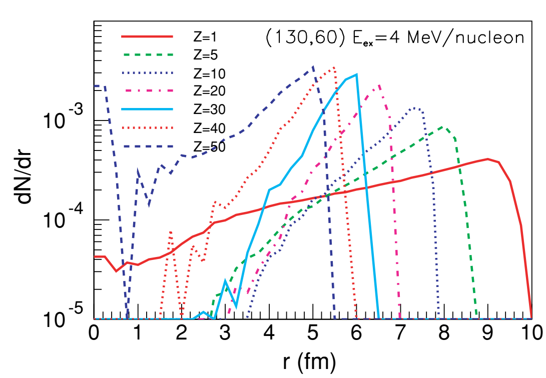

FIG. 5. (Color online) Radial probability distributions of different size ($Z = 1$, 5, 10, 20, 30, 40, and 50) primary fragments at break-up. The statistically equilibrated source (130, 60) is characterized by an excitation energy of 4 MeV/nucleon and a freeze-out volume $V = 6V_0$.

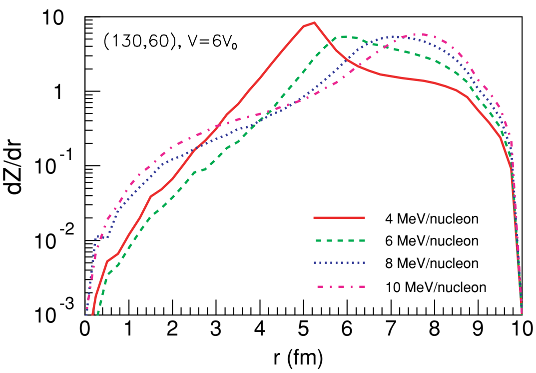

FIG. 6. (Color online) Total charge radial distributions corresponding to the (130,60) multifragmenting nucleus with $V = 6V_0$ and different excitation energies (4, 6, 8, and 10 MeV/nucleon).

the inner parts, while relatively light nuclei may be created over wider regions. This means that the lighter the fragment, the stronger is the Coulomb repulsion the charged core will exercise over it, and consequently the higher is its final kinetic energy. This explains the observed systematic shift between the maximum values of kinetic energy corresponding to the three largest fragments. The systematic reduction of the volume accessible to a fragment as its mass increases is the consequence of the employed nonoverlapping condition between a fragment and the wall of the container which mimics the freeze-out volume. For the heaviest fragments ($Z = 50$), this geometric condition is responsible for fragment concentration in a region that represents only 15% of the total freeze-out volume. We recall that the classification of multifragmentation events with respect to fragments' spatial arrangement and its influence on fragment-fragment correlation functions was discussed for the first time in Ref. [20] in the framework of the Microcanonical Metropolis-Monte Carlo (MMMC) model [3], in which the authors identified "sun"- and "soup"-like events.

As the source excitation energy increases and fragmentation becomes more advanced, a more uniform population of the freeze-out volume is expected, such that the largest fragments' kinetic energy shifts become negligible. The evolution of the total charge radial distribution with source excitation is illustrated in Fig. 6 for the same multifragmenting nucleus (130, 60) with $V = 6V_0$. Indeed, at 8 MeV/nucleon, the matter in the inner regions of the freeze-out volume is 10 times denser that the one produced at 6 MeV/nucleon, but the overall distribution remains strongly outward peaked, giving the source a bubble-like structure. Bubble-like structures of the nuclear matter at break-up have been obtained also in the framework of stochastic mean-field approaches [21], which explain fragmentation on behalf of growing volume and surface instabilities encountered during the expansion phase of the excited system, as recently reported in Refs. [22,23]. This agreement between results of statistical models with cluster degrees of freedom and dynamical models with nucleonic degrees of freedom is far from being trivial taking into account the conceptually different scenarios the two categories of models advance for explaining multifragmentation and the almost complementary treatment of the physical process.

V. CONCLUSIONS

To conclude, using a microcanonical multifragmentation model with cluster degrees of freedom, we have analyzed the break-up fragmentation patterns of a medium size equilibrated source that follows different paths through the excitation-energy–freeze-out volume space. The constraints imposed on the freeze-out volume are found to not affect significantly the magnitude of different energy fluctuations. Moreover, kinetic and configurational energy fluctuations are insensitive to the system phase properties as long as the considered fragment partitions are similar. Over the whole domain of excitation energy, spatial matter distribution at break-up is highly nonuniform, its outward-peaked shape giving the source a bubble-like structure. The most probable localization of nuclear fragments at break-up depends on fragment mass, and because of Coulomb acceleration, it is possible to infer it from the experimentally accessible fragment average kinetic energy distributions, especially at intermediate values of source excitation. Thus, heavy fragments are found to be produced in the inner regions of the freeze-out volume, while the lighter ones are produced in a larger region of the freeze-out volume. Considering that break-up fragments interact not only through repulsive hard-core and Coulomb potentials but also via proximity potentials, one obtains dramatic modifications of the break-up fragmentation patterns, which suggest that final fragment formation is strongly influenced by post-break-up dynamics and multiparticle correlations.

ACKNOWLEDGMENTS

The author acknowledges partial support from the Romanian National Authority for Scientific Research under the PNCDI2 programme, Grant IDEI nr. 267/2007.

[1] *Special Issue: Dynamics and Thermodynamics with Nuclear Degrees of Freedom*, Eur. Phys. J. A **30**, No. 1 (2006).
[2] B. Borderie and M. F. Rivet, Prog. Part. Nucl. Phys. **61**, 551 (2008).
[3] D. H. E. Gross, Rep. Prog. Phys. **53**, 605 (1990).
[4] J. P. Bondorf, A. S. Botvina, A. S. Iljinov, I. N. Mishustin, and K. Sneppen, Phys. Rep. **257**, 133 (1995).
[5] S. E. Koonin and J. Randrup, Nucl. Phys. **A474**, 173 (1987).
[6] Al. H. Raduta and Ad. R. Raduta, Phys. Rev. C **55**, 1344 (1997).
[7] S. Das Gupta and A. Z. Mekjian, Phys. Rev. C **57**, 1361 (1998); S. Pratt and S. Das Gupta, *ibid.* **62**, 044603 (2000).
[8] Al. H. Raduta and Ad. R. Raduta, Phys. Rev. C **65**, 054610 (2002).
[9] Ad. R. Raduta, E. Bonnet, B. Borderie, N. Le Neindre, and M. F. Rivet, Phys. Rev. C **72**, 057603 (2005).
[10] M. B. Tsang *et al.*, Eur. Phys. J. A **30**, 129 (2006).
[11] S. Pal, S. K. Samaddar, A. Das, and J. N. De, Nucl. Phys. **A586**, 466 (1995).

[12] S. K. Samaddar, J. N. De, and A. Bonasera, Phys. Rev. C **71**, 011601(R) (2005).
[13] D. H. E. Gross and E. Votyakov, Eur. Phys. J. B **15**, 115 (2000).
[14] D. H. E. Gross, Nucl. Phys. **A681**, 366 (2001).
[15] L. Satpathy, M. Mishra, A. Das, and M. Satpathy, Phys. Lett. **B237**, 181 (1990).
[16] S. Piantelli *et al.*, Nucl. Phys. **A809**, 111 (2008).
[17] E. Bonnet and the INDRA Collaboration, Nucl. Phys. **A816**, 1 (2009).
[18] Ad. R. Raduta, B. Borderie, E. Bonnet, N. Le Neindre, S. Piantelli, and M. F. Rivet, Phys. Lett. **B623**, 43 (2005).
[19] G. Tabacaru *et al.*, Nucl. Phys. **A764**, 371 (2006).
[20] O. Schapiro and D. H. E. Gross, Nucl. Phys. **A576**, 428 (1994).
[21] A. Guarnera, M. Colonna, and Ph. Chomaz, Phys. Lett. **B373**, 267 (1996); M. Colonna *et al.*, Nucl. Phys. **A642**, 449 (1998).
[22] M. Parlog, G. Tabacaru, J. P. Wieleczko, J. D. Frankland, B. Borderie, A. Chbihi, M. Colonna, and M. F. Rivet, Eur. Phys. J. A **25**, 223 (2005).
[23] M. Colonna, G. Fabbri, M. Di Toro, F. Matera, and H. H. Wolter, Nucl. Phys. **A742**, 337 (2004).